Catalysis Today 146 (2009) 44–49

Contents lists available at ScienceDirect

Catalysis Today

journal homepage: www.elsevier.com/locate/cattod

Hydrogen production by steam reforming of liquefied natural gas (LNG) over mesoporous nickel–alumina composite catalyst prepared by an anionic surfactant-templating method

Jeong Gil Seo [a], Min Hye Youn [a], Sunyoung Park [a], Dong Ryul Park [a], Ji Chul Jung [a], Jin Suk Chung [b], In Kyu Song [a,*]

[a] School of Chemical and Biological Engineering, Research Center for Energy Conversion and Storage, Seoul National University, Shinlim-dong, Kwanak-ku, Seoul 151-744, South Korea
[b] School of Chemical Engineering and Bioengineering, University of Ulsan, Ulsan 680-749, South Korea

ARTICLE INFO

Article history:
Available online 18 January 2009

Keywords:
Nickel–alumina catalyst
Anionic surfactant
Liquefied natural gas
Steam reforming
Hydrogen production

ABSTRACT

A mesoporous nickel–alumina composite catalyst (Ni–Al_2O_3) was prepared by an anionic surfactant-templating method, and was applied to hydrogen production by steam reforming of liquefied natural gas (LNG). For comparison, a nickel catalyst supported on mesoporous alumina (Ni/Al_2O_3) was prepared by an impregnation method. High surface area and well-developed mesopores of both Ni–Al_2O_3 and Ni/Al_2O_3 catalysts improved the dispersion of nickel species through the formation of nickel aluminate phase. In the Ni–Al_2O_3 catalyst, nickel species were homogeneously dispersed without significant pore blocking through the formation of Ni–O–Al composite structure. The Ni–Al_2O_3 catalyst was very efficient for suppressing the nickel sintering during the reduction process, resulting in enhanced nickel dispersion and active nickel surface area. Ni–Al_2O_3 catalyst showed a stable catalytic performance without significant catalyst deactivation during the reaction extending over 3000 min, while Ni/Al_2O_3 catalyst exhibited a stable catalytic performance at the initial stage but experienced a slight catalyst deactivation in the long run. The Ni–Al_2O_3 catalyst showed a better catalytic performance than the Ni/Al_2O_3 catalyst. High active nickel surface area and fine nickel dispersion of Ni–Al_2O_3 catalyst played an important role in enhancing the dehydrogenation reaction of hydrocarbon species and the gasification reaction of adsorbed carbon species in the steam reforming of LNG. Strong resistance of Ni–Al_2O_3 catalyst toward carbon deposition and nickel sintering was also responsible for its high catalytic performance.

1. Introduction

Development of new and clean energy has been widely studied because of the high price of fossil fuels and associated environmental problems [1]. In particular, hydrogen has attracted much attention as an alternative energy source due to its clean, renewable, and non-polluting nature [2]. Several catalytic processes for the production of hydrogen from hydrocarbons and alcohols have been investigated, including steam reforming [3–7], partial oxidation [8,9], auto-thermal reforming [10–12], and CO_2 reforming [13,14]. Among these catalytic reforming technologies, steam reforming has been recognized as the most feasible process for converting methane into hydrogen. Liquefied natural gas (LNG), which is abundant and mainly composed of methane, can serve as a promising source for hydrogen production by steam reforming reaction. LNG pipelines may become more widespread in the future, which will make LNG well suited as a hydrogen source for residential reformers in fuel cell applications. Sulfur-free nature of LNG also lessens the significant concern about environmental contamination and catalyst poisoning caused by sulfur compounds.

It is known that both palladium-based and nickel-based catalysts exhibit a high catalytic performance in the steam reforming reactions [15,16]. However, the palladium-based catalysts are disadvantageous in hydrogen production by steam reforming reaction due to their high price. Although the nickel-based catalysts have many advantages over the palladium-based catalysts in hydrogen production by steam reforming reactions due to their low cost and relatively high catalytic activity, the nickel-based catalysts require high reaction temperatures and excess amounts of steam to prevent nickel sintering and carbon deposition on the catalyst surface during the reactions [17–20].

Many efforts have been made to increase the stability of nickel-based catalysts in the steam reforming reactions [21–25]. In

* Corresponding author. Tel.: +82 2 880 9227; fax: +82 2 889 7415.
E-mail address: inksong@snu.ac.kr (I.K. Song).

0920-5861/$ – see front matter © 2008 Elsevier B.V. All rights reserved.
doi:10.1016/j.cattod.2008.12.008

general, the catalytic performance of nickel-based catalysts strongly depends not only on the nature of active nickel, but also on the chemical and physical properties of supporting material. Therefore, modification of supporting material has been attempted as one of the promising approaches to achieve high catalytic performance of nickel-based catalysts. For example, it was reported that mesoporous alumina supports greatly enhanced the coking resistance of nickel-based catalysts in the reforming reactions by improving the active nickel surface area [4,14,26,27].

It has been reported that mesoporous aluminas with high surface area and narrow pore size distribution can be synthesized by a templating method using anionic [9,28–30], cationic [28,31,32], and non-ionic [33,34] surfactants. Among various surfactants, the anionic surfactant is known as a suitable template for the preparation of mesoporous metal–alumina composite catalyst, which can be obtained via the formation of (metal precursor)$^{+}$(anionic surfactant)$^{-}$(aluminum precursor)$^{+}$. However, the surfactant-templated mesoporous nickel–alumina composite has never been used as a catalyst for the reforming reactions. Therefore, developing an anionic surfactant-templated mesoporous nickel–alumina composite catalyst for hydrogen production by steam reforming of LNG would be of great interest.

In this work, a mesoporous nickel–alumina composite catalyst was prepared by an anionic surfactant-templating method, and was applied to hydrogen production by steam reforming of LNG. For comparison, a nickel catalyst supported on mesoporous alumina was prepared by an impregnation method. The effect of nickel dispersion and nickel surface area on the catalytic performance in the steam reforming of LNG was investigated. It is expected that pore blocking by nickel species, which is unavoidable in the preparation of nickel catalyst supported on mesoporous alumina by a conventional impregnation method, would be significantly suppressed in the mesoporous nickel–alumina composite catalyst.

2. Experimental

2.1. Preparation of mesoporous nickel–alumina composite catalyst

A mesoporous nickel–alumina composite catalyst was prepared by an anionic surfactant-templating method, according to the similar methods reported in literature [9,28]. 3 g of anionic surfactant (lauric acid, Sigma–Aldrich) was dissolved in 30 ml of 1-propanol (Sigma–Aldrich) at room temperature under constant stirring to yield a micelle solution (solution A). 17.4 g of aluminum precursor (aluminum *sec*-butoxide, Sigma–Aldrich) was then separately dissolved in 30 ml of 1-propanol at room temperature under constant stirring (solution B). After adding solution B to solution A, the resulting solution was stirred for 2 h to obtain a micelle-aluminum precursor complex (solution C). Another solution containing 3.6 g of nickel precursor (nickel nitrate hexahydrate, Sigma–Aldrich) and 2.75 ml of distilled water was diluted with 17.5 ml of 1-propanol (solution D). A semi-solid solution of nickel precursor–micelle–aluminum precursor complex was formed within a few seconds upon adding the solution D into the solution C. After stirring the semi-solid solution for 2 h, it was maintained at 100 °C for 24 h. The solid obtained by centrifugation was successively washed with ethanol and distilled water. The solid product was dried overnight at 100 °C, and then it was calcined at 700 °C for 5 h to yield the mesoporous nickel–alumina composite catalyst. The mesoporous nickel–alumina composite catalyst was denoted as Ni–Al_2O_3.

A mesoporous alumina was prepared according to the reported method [28] for use as a supporting material (simply denoted as Al_2O_3). A nickel catalyst supported on afore-mentioned mesoporous alumina (Al_2O_3) was then prepared by impregnating a known amount of nickel precursor (nickel nitrate hexahydrate, Sigma–Aldrich) on Al_2O_3 for comparison and reference. The nickel catalyst supported on mesoporous alumina was denoted as Ni/Al_2O_3.

2.2. Characterization

Nitrogen adsorption–desorption isotherms of support (Al_2O_3) and catalysts (Ni–Al_2O_3 and Ni/Al_2O_3) were obtained with an ASAP-2010 (Micromeritics) instrument, and pore size distributions of support (Al_2O_3) and catalysts (Ni–Al_2O_3 and Ni/Al_2O_3) were determined by the Barret–Joyner–Hallender (BJH) method applied to the desorption branches of nitrogen isotherms. Crystalline phases of support (Al_2O_3) and catalysts (Ni–Al_2O_3 and Ni/Al_2O_3) were investigated by XRD (D-Max2500-PC, Rigaku) measurements using Cu Kα radiation (λ = 1.541 Å) operated at 50 kV and 100 mA. In order to examine the reducibility of the catalysts, temperature-programmed reduction (TPR) measurements were carried out in a conventional flow system with a moisture trap connected to a thermal conductivity detector (TCD) at temperatures ranging from room temperature to 1000 °C with a ramping rate of 5 °C/min. For the TPR measurements, a mixed stream of H_2 (2 ml/min) and N_2 (20 ml/min) was used for 0.1 g of catalyst sample. Hydrogen chemisorption experiments (BELCAT-B, BEL Japan) were conducted to measure the nickel dispersion and nickel surface area of the catalysts. Prior to the chemisorption measurements, 50 mg of each catalyst was reduced with a mixed stream of hydrogen (2.5 ml/min) and argon (47.5 ml/min) at 700 °C for 3 h, and subsequently, it was purged with pure argon (50 ml/min) for 15 min at 700 °C. The sample was then cooled to 50 °C under a flow of argon (50 ml/min). The amount of hydrogen uptake was determined by periodically injecting diluted hydrogen (5% hydrogen and 95% argon) into the reduced catalyst using an on-line sampling valve. Nickel dispersion and nickel surface area were calculated by assuming that one hydrogen atom occupies one surface nickel atom and that cross-sectional area of atomic nickel is 6.49×10^{-20} m^2/Ni-atom. TEM analyses (JEM-2000EXII, JEOL) were conducted to examine the nickel dispersion on the reduced catalysts. Carbon deposition in the used catalysts was determined by CHNS elemental analyses (CHNS 932, Leco).

2.3. Steam reforming of LNG

Steam reforming of LNG was carried out in a continuous flow fixed-bed reactor at 600 °C under atmospheric pressure. Prior to the catalytic reaction, each catalyst (100 mg) was reduced with a mixed stream of H_2 (3 ml/min) and N_2 (30 ml/min) at 700 °C for 3 h. Feed composition was fixed at CH_4:C_2H_6:H_2O:N_2 = 4.6:0.4:10:30, and total feed rate with respect to catalyst weight was maintained at 27,000 ml/h g-catalyst. Reaction products were periodically sampled and analyzed using an on-line gas chromatograph (ACME 6000, Younglin) equipped with a TCD. LNG conversion and product composition in dry gas were calculated according to the following equations on the basis of carbon balance:

$$\text{LNG conversion}\ (\%) = \left(1 - \frac{F_{CH_4,out} + F_{C_2H_6,out}}{F_{CH_4,in} + F_{C_2H_6,in}}\right) \times 100 \quad (1)$$

$$\text{Product composition in dry gas}\ (\%) = \frac{F_{product,out}}{F_{H_2,out} + F_{CH_4,out} + F_{C_2H_6,out} + F_{CO,out} + F_{CO_2,out}} \times 100 \quad (2)$$

3. Results and discussion

3.1. Chemical and physical properties

Textural properties of support and catalysts were examined by nitrogen adsorption–desorption isotherm measurements. Fig. 1(a)

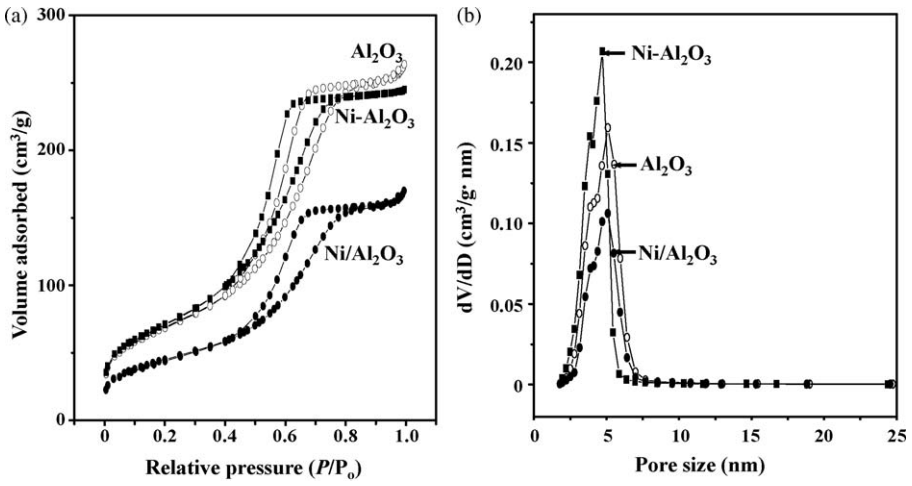

Fig. 1. (a) Nitrogen adsorption–desorption isotherms, and (b) BJH pore size distributions of Al_2O_3, Ni/Al_2O_3, and $Ni–Al_2O_3$ obtained from desorption branches.

shows the nitrogen adsorption–desorption isotherms of Al_2O_3, Ni/Al_2O_3, and $Ni–Al_2O_3$. It was observed that all the samples retained typical IV-type isotherm with H2-type hysteresis loop, indicating the existence of well-developed mesopores [35,36]. Fig. 1(b) shows the BJH pore size distributions of Al_2O_3, Ni/Al_2O_3, and $Ni–Al_2O_3$ obtained from desorption branches. All the samples exhibited narrow pore size distribution centered at around 4–4.5 nm.

Detailed chemical and physical properties of Al_2O_3, Ni/Al_2O_3, and $Ni–Al_2O_3$ are summarized in Table 1. It is interesting to note that surface area, pore volume, and average pore diameter of $Ni–Al_2O_3$ were quite different from those of Ni/Al_2O_3, although Ni/Al atomic ratio in both catalysts was almost identical. It was also revealed that the Ni/Al_2O_3 catalyst exhibited smaller surface area and pore volume than the Al_2O_3 support, in good agreement with the previous reports [14,27,37]. This result indicates that mesopores of Al_2O_3 support were significantly blocked by the nickel species during the preparation of Ni/Al_2O_3 catalyst by an impregnation method. On the other hand, the $Ni–Al_2O_3$ catalyst retained high surface area and large pore volume compared to the Ni/Al_2O_3 catalyst. Furthermore, surface area and pore volume of $Ni–Al_2O_3$ were comparable to those of Al_2O_3. This means that nickel species were homogeneously dispersed in the $Ni–Al_2O_3$ catalyst. It can be inferred that micelle with anionic charge was successfully bonded to positively charged nickel precursor and aluminum precursor in the preparation of $Ni–Al_2O_3$ catalyst. This $(\text{nickel precursor})^+(\text{micelle})^-(\text{aluminum precursor})^+$ complex was then transformed into the Ni–O–Al composite material upon removal of surfactant through the calcination process.

3.2. Crystal structure

Fig. 2 shows the XRD patterns of Al_2O_3, Ni/Al_2O_3, and $Ni–Al_2O_3$ calcined at 700 °C for 5 h. Al_2O_3 support showed the characteristic diffraction peaks of γ-alumina. It is noticeable that no characteristic diffraction peaks corresponding to nickel oxide were observed in both Ni/Al_2O_3 and $Ni–Al_2O_3$ catalysts. This indicates that nickel species were finely dispersed in the Ni/Al_2O_3 and $Ni–Al_2O_3$ catalysts, by forming small nickel particles that were under the detection limit of XRD measurements. On the other hand, diffraction peaks (solid lines) indicative of nickel aluminate ($NiAl_2O_4$) phase were observed in both Ni/Al_2O_3 and $Ni–Al_2O_3$ catalysts. The formation of nickel aluminate phase in both catalysts was attributed to the lattice expansion of γ-Al_2O_3 caused by the incorporation of Ni^{2+} into the lattice of γ-Al_2O_3 [38–40]. The formation of nickel aluminate phase in the Ni/Al_2O_3 and $Ni–Al_2O_3$ catalysts was also evidenced by the shift of (4 4 0) diffraction peak of alumina to lower diffraction angle. It is believed that nickel aluminate phase was formed in both Ni/Al_2O_3 and $Ni–Al_2O_3$ catalysts due to the homogeneous mixing and interaction between alumina and nickel species.

Table 1
Chemical and physical properties of Al_2O_3, Ni/Al_2O_3, and $Ni–Al_2O_3$.

Sample	Ni/Al atomic ratio[a]	Surface area (m^2/g)[b]	Pore volume (cm^3/g)[c]	Average pore diameter (nm)[d]
$Ni–Al_2O_3$	0.35	259	0.38	4.0
Al_2O_3	–	250	0.40	4.5
Ni/Al_2O_3	0.36	163	0.25	4.5

[a] Determined by ICP-AES measurement.
[b] Calculated by the BET equation.
[c] BJH desorption pore volume.
[d] BJH desorption average pore diameter.

3.3. Metal-support interaction

TPR measurements were carried out to investigate the reducibility of Ni/Al_2O_3 and $Ni–Al_2O_3$ catalysts and to examine

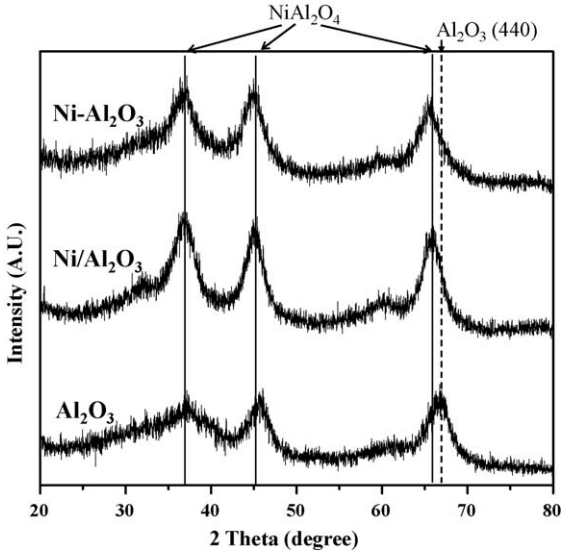

Fig. 2. XRD patterns of Al_2O_3, Ni/Al_2O_3, and $Ni–Al_2O_3$ calcined at 700 °C for 5 h.

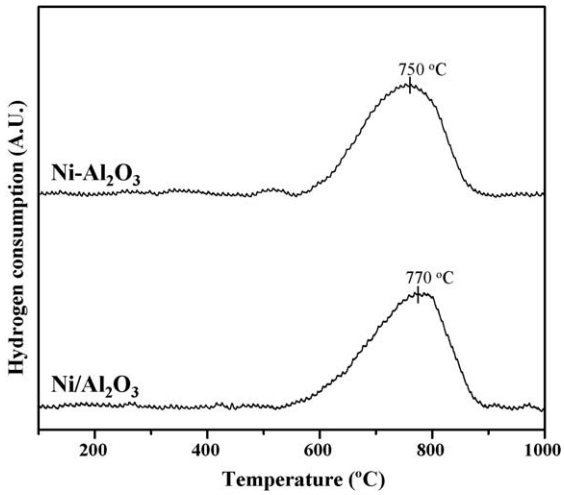

Fig. 3. TPR profiles of Ni/Al_2O_3 and $Ni–Al_2O_3$ catalysts.

Table 2
Hydrogen chemisorption results for $Ni–Al_2O_3$ and Ni/Al_2O_3 catalysts.

Hydrogen chemisorption results	$Ni–Al_2O_3$	Ni/Al_2O_3
Amount of hydrogen uptake (μmol/g-catalyst)	46.6	21.7
Nickel dispersion (%)[a]	3.6	1.7
Nickel surface area (m^2/g-Ni)[a]	23.9	11.1

[a] Calculated by assuming $H/Ni_{atom} = 1$.

the interaction between nickel species and alumina. TPR profiles of supported nickel catalysts are strongly affected by the nature of metal-support interaction. Fig. 3 shows the TPR profiles of Ni/Al_2O_3 and $Ni–Al_2O_3$ catalysts. Reduction bands of bulk nickel oxide species, which normally appeared in low temperature region (<600 °C), were not observed in both catalysts. Instead, both Ni/Al_2O_3 and $Ni–Al_2O_3$ catalysts showed the typical reduction profiles of nickel aluminate phase with no great difference in TPR peak temperature [41–43]. This result was in good agreement with the XRD result (Fig. 2).

3.4. Nickel dispersion and nickel surface area

Hydrogen chemisorption measurements were conducted in order to determine the nickel dispersion and nickel surface area in the $Ni–Al_2O_3$ and Ni/Al_2O_3 catalysts. In the hydrogen chemisorption measurements, it is known that a number of variables, such as adsorption temperature, adsorption pressure, pretreatment condition, and preparation method, affect the amount of hydrogen uptake on the nickel surface [44–46]. Furthermore, adsorption stoichiometry factor (H/Ni_{atom}), which is a very important parameter in the calculation of nickel dispersion and nickel surface area, is significantly influenced by the physico-chemical properties of the catalyst.

Hydrogen chemisorption results for $Ni–Al_2O_3$ and Ni/Al_2O_3 catalysts are listed in Table 2. It was observed that the amount of hydrogen uptake on the surface of $Ni–Al_2O_3$ catalyst was about two times larger than that on the surface of Ni/Al_2O_3 catalyst. It can be inferred from this result that nickel species were more finely dispersed in the $Ni–Al_2O_3$ catalyst through the formation of Ni–O–Al composite structure. Other effects can be negligible because both $Ni–Al_2O_3$ and Ni/Al_2O_3 catalysts retained almost identical Ni/Al atomic ratio (Table 1), crystalline structure (Fig. 2), and metal-support interaction (Fig. 3). Table 2 clearly shows that the $Ni–Al_2O_3$ catalyst was very efficient for suppressing the nickel sintering during the reduction process, resulting in its enhanced nickel dispersion and nickel surface area compared to the Ni/Al_2O_3 catalyst.

The above result was further confirmed by TEM analyses. Fig. 4 shows the TEM images of Ni/Al_2O_3 and $Ni–Al_2O_3$ catalysts reduced at 700 °C for 3 h. Compared to the Ni/Al_2O_3 catalyst, the $Ni–Al_2O_3$ catalyst retained finely dispersed metallic nickel species, in good agreement with the hydrogen chemisorption results (Table 2).

3.5. Catalytic performance in the steam reforming of LNG

Fig. 5 shows the LNG conversions with time on stream in the steam reforming of LNG over Ni/Al_2O_3 and $Ni–Al_2O_3$ catalysts at 600 °C. $Ni–Al_2O_3$ catalyst showed a stable catalytic performance without significant catalyst deactivation during the reaction extending over 3000 min, while Ni/Al_2O_3 catalyst exhibited a stable catalytic performance at the initial stage but experienced a slight catalyst deactivation in the long run. This means that both $Ni–Al_2O_3$ and Ni/Al_2O_3 catalysts can serve as potentially available catalysts for hydrogen production by steam reforming of LNG. Relatively stable catalytic performance of both catalysts can be explained by their favorable chemical and physical properties. Well-developed mesopores and finely dispersed nickel species in both $Ni–Al_2O_3$ and Ni/Al_2O_3 catalysts effectively suppressed the carbon deposition and nickel sintering through an acceleration of gasification reaction between adsorbed intermediate carbon species and adsorbed steam ($–OH_2$) or hydroxyl molecules (–OH). However, it was observed that the $Ni–Al_2O_3$ catalyst showed a better catalytic performance than the Ni/Al_2O_3 catalyst. This might

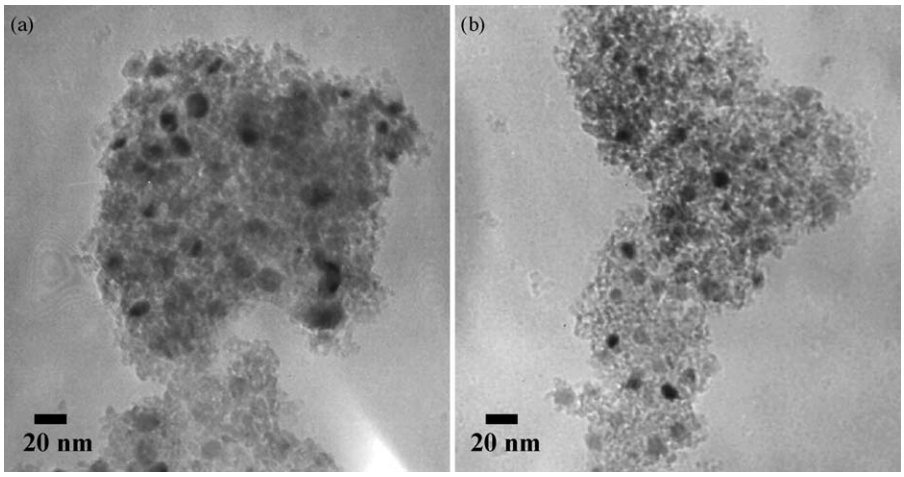

Fig. 4. TEM images of (a) Ni/Al_2O_3 and (b) $Ni–Al_2O_3$ catalysts reduced at 700 °C for 3 h.

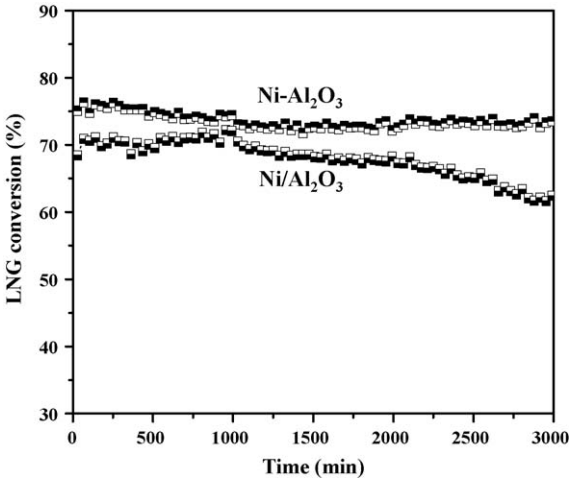

Fig. 5. LNG conversions with time on stream in the steam reforming of LNG over Ni/Al_2O_3 and Ni–Al_2O_3 catalysts at 600 °C. All the catalysts were reduced at 700 °C prior to the reaction.

be due to the fact that the Ni–Al_2O_3 catalyst retained high nickel dispersion and high active nickel surface area compared to the Ni/Al_2O_3 catalyst (Table 2).

Hydrogen production by steam reforming of methane over nickel-based catalysts is closely related to the following adsorption mechanisms [47–49]. One is the dissociate adsorption of methane on the active nickel surface (Eq. (3)), and the other is the dissociate adsorption of steam on either the active nickel surface (Eq. (4)) or the support (Eq. (5)). Here, Ni_s and S_s represent adsorption site on the surface of nickel and support, respectively:

$$CH_4 + Ni_s \leftrightarrow CH_2{-}Ni_s + H_2 \quad (3)$$

$$H_2O + Ni_s \leftrightarrow O{-}Ni_s + H_2 \quad (4)$$

$$H_2O + S_s \leftrightarrow H_2O{-}S_s \quad (5)$$

Steam adsorbed on the surface of support readily undergoes spillover onto the surface of active nickel site (Eq. (6)):

$$H_2O{-}S_s + Ni_s \leftrightarrow Ni_s{-}O + S_s + H_2 \quad (6)$$

The catalytic performance of supported nickel catalysts, therefore, is strongly affected not only by the number of active nickel site, but also by the number of nearby active support site. This means that chemical and physical modifications of nickel species and supporting material are very important to enhance the steam reforming performance of supported nickel catalysts. In other words, the steam reforming reaction composed of dehydrogenation reaction of hydrocarbon species and gasification reaction of adsorbed carbon species can be preferentially enhanced by improving the dispersion of active nickel site on the catalyst surface. Therefore, it is inferred from Table 2 that the Ni–Al_2O_3 catalyst showed a better catalytic performance that the Ni/Al_2O_3 catalyst in the steam reforming of LNG.

Typical catalytic performance of Ni–Al_2O_3 and Ni/Al_2O_3 catalysts in the steam reforming of LNG after a 1500 min reaction is listed in Table 3. The Ni–Al_2O_3 catalyst exhibited a better catalytic performance than the Ni/Al_2O_3 catalyst in terms of LNG conversion and H_2 composition in dry gas. Furthermore, the Ni–Al_2O_3 catalyst showed higher H_2/CO and CO_2/CO ratios than the Ni/Al_2O_3 catalyst. This result indicates that water–gas shift reaction (Eq. (7)) was accelerated during the steam reforming reaction over the Ni–Al_2O_3 catalyst rather than over the Ni/Al_2O_3 catalyst:

$$H_2O + CO \leftrightarrow CO_2 + H_2 \quad (7)$$

Table 3
Typical catalytic performance of Ni–Al_2O_3 and Ni/Al_2O_3 catalysts in the steam reforming of LNG after a 1500 min reaction.

Catalytic performance	Ni–Al_2O_3	Ni/Al_2O_3
LNG conversion (%)	72.7	68.2
H_2 composition in dry gas (%)	66.4	65.3
CO composition in dry gas (%)	11.8	12.5
CO_2 composition in dry gas (%)	14.9	13.8
H_2/CO ratio	5.61	5.21
CO_2/CO ratio	1.26	1.10

3.6. Characterization of used catalysts

Fig. 6 shows the XRD patterns of Ni–Al_2O_3 and Ni/Al_2O_3 catalysts obtained after a 3000 min reaction at 600 °C. Both Ni–Al_2O_3 and Ni/Al_2O_3 catalysts retained metallic nickel species (dashed lines). However, neither nickel oxide species nor nickel aluminate phase was detected in both used Ni–Al_2O_3 and Ni/Al_2O_3 catalysts. This means that nickel species in both catalysts were readily reduced into metallic nickel during the reduction process, and their electronic state still remained without change during the reaction. It is interesting to note that graphitic carbon species were observed in the used Ni/Al_2O_3 catalyst.

Characterization results for Ni–Al_2O_3 and Ni/Al_2O_3 catalysts obtained after a 3000 min reaction at 600 °C are listed in Table 4. It is noticeable that the Ni–Al_2O_3 catalyst showed a smaller nickel crystalline size than the Ni/Al_2O_3 catalyst. Moreover, the amount of carbon deposition on the Ni–Al_2O_3 catalyst was smaller than that on the Ni/Al_2O_3 catalyst. It has been reported that nickel catalysts activate both steam reforming reaction and carbon formation reaction [50]. Carbon deposition reaction preferentially occurs on the surface of large nickel particles, and small nickel particles have strong resistance toward carbon deposition [50]. Therefore, it is concluded that the Ni–Al_2O_3 composite catalyst prepared by an anionic surfactant-templating method exhibited an excellent catalytic performance by enhancing the steam reforming reaction between hydrocarbon and steam and by suppressing the carbon deposition and nickel sintering.

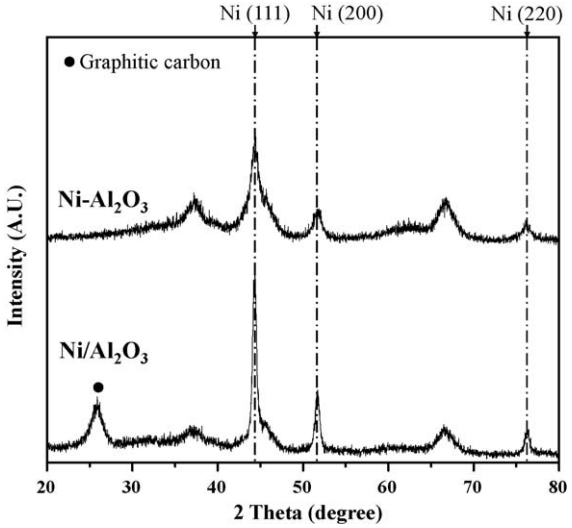

Fig. 6. XRD patterns of Ni/Al_2O_3 and Ni–Al_2O_3 catalysts obtained after a 3000 min reaction at 600 °C.

Table 4
Characterization results for Ni–Al_2O_3 and Ni/Al_2O_3 catalysts obtained after a 3000 min reaction at 600 °C.

Catalyst	Ni crystalline size (nm)[a]	Amount of carbon deposition (wt%)[b]
Ni–Al_2O_3	7.5	1.4
Ni/Al_2O_3	14.5	20.8

[a] Calculated from Ni (2 2 0) diffraction peak broadening in Fig. 6.
[b] Determined by CHNS elemental analysis.

4. Conclusions

Ni–Al_2O_3 catalyst was prepared by an anionic surfactant-templating method, and was applied to hydrogen production by steam reforming of LNG. Ni/Al_2O_3 catalyst was also prepared by an impregnation method for comparison. The effect of nickel dispersion and nickel surface area on the catalytic performance of Ni–Al_2O_3 and Ni/Al_2O_3 catalysts was investigated. It was revealed that high surface area and well-developed mesopores in both Ni–Al_2O_3 and Ni/Al_2O_3 catalysts improved the dispersion of nickel species through the formation of nickel aluminate phase. In particular, nickel species were homogeneously dispersed in the Ni–Al_2O_3 catalyst without significant pore blocking through the formation of Ni–O–Al composite structure. The Ni–Al_2O_3 catalyst was very efficient for suppressing the nickel sintering during the reduction process, resulting in enhanced nickel dispersion and nickel surface area. Ni–Al_2O_3 catalyst showed a stable catalytic performance without significant catalyst deactivation during the reaction extending over 3000 min, while Ni/Al_2O_3 catalyst exhibited a stable catalytic performance at the initial stage but experienced a slight catalyst deactivation in the long run. The Ni–Al_2O_3 catalyst showed a better catalytic performance than the Ni/Al_2O_3 catalyst. High nickel dispersion and high active nickel surface area of Ni–Al_2O_3 catalyst played an important role in enhancing the dehydrogenation reaction of hydrocarbon species and the gasification reaction of adsorbed carbon species in the steam reforming of LNG. The Ni–Al_2O_3 composite catalyst prepared by an anionic surfactant-templating method exhibited a superior catalytic performance by enhancing the steam reforming reaction between hydrocarbon and steam and by suppressing the carbon deposition and nickel sintering.

Acknowledgements

The authors wish to acknowledge support from the Seoul Renewable Energy Research Consortium (Seoul R & BD Program) and RCECS (Research Center for Energy Conversion and Storage: R11-2002-102-00000-0).

References

[1] M. Schrope, Nature 414 (2001) 682.
[2] J.N. Armor, Appl. Catal. A 176 (1999) 159.
[3] Q. Ming, T. Healey, L. Allen, P. Irving, Catal. Today 77 (2002) 51.
[4] J.G. Seo, M.H. Youn, K.M. Cho, S. Park, S.H. Lee, J. Lee, I.K. Song, Korean J. Chem. Eng. 25 (2008) 41.
[5] J.G. Seo, M.H. Youn, S. Park, J. Lee, S.H. Lee, H. Lee, I.K. Song, Korean J. Chem. Eng. 25 (2008) 95.
[6] J.D. Ko, J.K. Lee, D. Park, S.H. Shin, Korean J. Chem. Eng. 12 (1995) 478.
[7] K.J. Lee, D. Park, Korean J. Chem. Eng. 15 (1998) 658.
[8] X.X. Gao, C.J. Huang, N.W. Zhang, J.H. Li, W.Z. Weng, H.L. Wan, Catal. Today 131 (2008) 211.
[9] P. Kim, Y. Kim, H. Kim, I.K. Song, J. Yi, Appl. Catal. A 272 (2004) 157.
[10] T. Takeguchi, S.-N. Furukawa, M. Inoue, K. Eguchi, Appl. Catal. A 240 (2003) 223.
[11] X. Cai, X. Dong, W. Lin, J. Nat. Gas Chem. 15 (2006) 122.
[12] M.H. Youn, J.G. Seo, K.M. Cho, J.C. Jung, H. Kim, K.W. La, D.R. Park, S. Park, S.H. Lee, I.K. Song, Korean J. Chem. Eng. 25 (2008) 236.
[13] A. Nandini, K.K. Pant, S.C. Dhingra, Appl. Catal. A 308 (2006) 119.
[14] J.-H. Kim, D.J. Suh, T.-J. Park, K.-L. Kim, Appl. Catal. A 197 (2000) 191.
[15] A.P.E. York, T. Xiao, M.L.H. Green, Top. Catal. 22 (2003) 345.
[16] P.K. Cheekatamarla, C.M. Finnerty, J. Power Sources 160 (2006) 490.
[17] J.R. Rostrup-Nielsen, J. Sehested, J.K. Nørskov, Adv. Catal. 47 (2002) 65.
[18] J.R. Rostrup-Nielsen, Catal. Today 63 (2000) 159.
[19] J. Sehested, A.P. Gelten, I.N. Remediakis, H. Bengaard, J.K. Nørskov, J. Catal. 223 (2004) 432.
[20] C.H. Bartholomew, R.B. Pannell, R.W. Fowler, J. Catal. 79 (1983) 34.
[21] T. Borowiecki, A. Gołębiowski, B. Stasińska, Appl. Catal. A 153 (1997) 141.
[22] T. Borowiecki, G. Wojciech, D. Andrzej, Appl. Catal. A 270 (2004) 27.
[23] L. Kępiński, B. Stasińska, T. Borowiecke, Carbon 38 (2000) 1845.
[24] J.G. Seo, M.H. Youn, I.K. Song, J. Mol. Catal. A 268 (2007) 9.
[25] J.S. Lisboa, D.C.R.M. Santos, F.B. Passos, F.B. Noronha, Catal. Today 101 (2005) 15.
[26] D.J. Suh, T.-J. Park, J.-H. Kim, K.-L. Kim, Chem. Mater. 9 (1997) 1903.
[27] J.G. Seo, M.H. Youn, K.M. Cho, S. Park, I.K. Song, J. Power Sources 173 (2007) 943.
[28] J.C. Ray, K.-S. You, J.-W. Ahn, W.-S. Ahn, Micropor. Mesopor. Mater. 100 (2007) 183.
[29] F. Vaurdy, S. Khodabandeh, M.E. Davis, Chem. Mater. 8 (1996) 1451.
[30] M. Yada, H. Hiyoshi, K. Ohe, M. Machida, T. Kijima, Inorg. Chem. 36 (1997) 5565.
[31] S. Valange, J.-L. Guth, F. Kolenda, S. Lacombe, Z. Gabelica, Micropor. Mesopor. Mater. 35 (2006) 597.
[32] H.C. Lee, H.J. Kim, C.H. Rhee, K.H. Lee, J.S. Lee, S.H. Chung, Micropor. Mesopor. Mater. 79 (2005) 61.
[33] S.A. Bagshaw, T.J. Pinnavaia, Angew. Chem. Int. Ed. 35 (1996) 1102.
[34] P. Yang, D. Zhao, D.I. Margolese, B.F. Chmelka, G.D. Stucky, Nature 396 (1998) 152.
[35] V. González-Peña, C. Márquez-Alvarez, I. Díaz, M. Grande, T. Blasco, J. Pérez-Pariente, Micropor. Mesopor. Mater. 80 (2005) 173.
[36] P.T. Tanev, T.J. Pinnavaia, Chem. Mater. 8 (1996) 2068.
[37] L. Pelletier, D.D.S. Liu, Appl. Catal. A 317 (2007) 293.
[38] J.A. Wang, A. Morales, X. Bokhimi, O. Novaro, Chem. Mater. 11 (1999) 308.
[39] E.D. Dimotakis, T.J. Pinnavaia, Inorg. Chem. 29 (1990) 2393.
[40] P. Kim, Y. Kim, H. Kim, I.K. Song, J. Yi, J. Mol. Catal. A 231 (2005) 247.
[41] O. Dewaele, G.F. Froment, J. Catal. 184 (1999) 499.
[42] J.M. Rynkowski, T. Paryczak, M. Lenik, Appl. Catal. A 106 (1992) 73.
[43] G. Li, L. Hu, J.M. Hill, Appl. Catal. A 310 (2006) 16.
[44] C.H. Bartholomew, R.B. Pannell, J. Catal. 65 (1980) 390.
[45] C. Hoang-Van, Y. Kachaya, S.J. Teichner, Appl. Catal. 46 (1989) 281.
[46] M.A. Vannice, J. Catal. 44 (1976) 152.
[47] Y. Matsumura, T. Nakamori, Appl. Catal. A 258 (2004) 107.
[48] K. Kochloefl, in: G. Ertl, H. Knözinger, J. Weitkamp (Eds.), Handbook of Heterogeneous Catalysis, vol. 4, Wiley, New York, 1997, pp. 1819–1831.
[49] J.R.H. Ross, M.C.F. Steel, A. Zeini-Asfanani (Eds.), Mechanisms of Hydrocarbon Reactions, Elsevier Science, Amsterdam, 1975, pp. 201–214.
[50] J.R. Rostrub-Nielson, D.L. Trimm, J. Catal. 48 (1977) 155.